https://doi.org/10.5194/egusphere-2026-6686
Preprint. Discussion started: 17 November 2026
© Author(s) 2026. CC BY 4.0 License.

A methodology to improve daytime passive microwave soil moisture retrievals

Dávid D.Kovács[1], Richard De Jeu[2], Colin Moldenhauer[1], Ruxandra-Maria Zotta[1], Nicolas François Bader[1], and Wouter Arnoud Dorigo[1]

[1]Department of Geodesy and Geoinformation, TU Wien, Wiedner Hauptstrasse 8, Vienna, 1040, Austria
[2]Transmissivity B.V., Alphen aan den Rijn, The Netherlands

Correspondence: Dávid D.Kovács (david.kovacs@tuwien.ac.at)

Abstract. Passive microwave radiometer observations are crucial for global soil moisture (SM) monitoring, yet daytime retrievals are affected from significant uncertainties. The radiometric observations used for SM retrieval are the product of both surface emissivity and effective temperature (T_{eff}). However, the precise estimation of T_{eff} is heavily affected by the strong vertical temperature gradients between the soil surface and the effective emitting layer. Accurate estimation of the emitting layer's T_{eff} during SM retrieval using radiative transfer schemes like the Land Parameter Retrieval Model is crucial. In LPRM T_{eff} is estimated by a globally generic approach using the vertically polarized Ka-band (TB_{KaV}), which measures only the topmost layer of the surface, however, SM estimation is done by lower frequencies like the C-band. Radiation at C-band is emitted from deeper soil layers as compared to what TB_{KaV} senses, causing a difference in the sensed temperatures, which becomes more apparent through the day, because strong solar illuminance heats up soil layers at different rates. The discrepancy between T_{eff} and surface temperature is a function of land cover type, which becomes particularly prominent in bare soils due to the significantly deeper penetration of lower frequencies compared to the Ka-band. To tackle this issue, we propose a novel approach: Globally, where the microwave polarization difference index (MPDI) is invariant from night-to-day, SM and vegetation optical depth (VOD) are assumed constant at this sub-daily timescale. Nighttime SM and VOD are then used as inputs to invert the radiative transfer equation and simulate T_{eff}. Linear regression between simulated T_{eff} and TB_{KaV} over time-invariant locations then yields slope and intercept maps. These globally variable regression slopes and intercepts are then used with TB_{KaV} to improve T_{eff} estimates which, as a consequence yield improved SM retrievals. The optimized daytime retrievals show globally reduced bias both on bare and vegetated land covers, when compared to nighttime retrievals and to ERA5-Land data. The method provides a robust bias reduction technique that can be used over multiple satellites for the C- and X-band frequencies.

1 Introduction

Over the years, passive microwave measurements from numerous satellite platforms have been used to derive surface soil moisture (SM). Besides the dedicated soil moisture missions, such as the Soil Moisture and Ocean Salinity (SMOS) mission of the European Space Agency (ESA) (Kerr et al., 2010) and the Soil Moisture Active Passive (SMAP) mission of the National

https://doi.org/10.5194/egusphere-2026-6686
Preprint. Discussion started: 17 November 2026
© Author(s) 2026. CC BY 4.0 License.

Aeronautics and Space Administration (Entekhabi et al., 2010), other platforms have also been used successfully to derive soil moisture. The available soil moisture retrievals using observations from the Advanced Microwave Scanning Radiometers (AMSR-E and AMSR2) are clear examples (Owe et al., 2008; Bindlish et al., 2017b; Meng et al., 2022). They have, in general, a lower quality compared to the retrievals from dedicated missions, but they remain very useful, particularly for the development of long-term climate data records (Wu et al., 2020; Du et al., 2017). The ESA Climate Change Initiative (CCI) SM program is one of the programs that harmonizes these records for the research community (Dorigo et al., 2017; Gruber et al., 2019). This effort has been ongoing for more than a decade, and the available datasets have demonstrated their value in scientific research, including studies on drought (Hirschi et al., 2025), water dynamics (van der Schalie et al., 2022; Dorigo et al., 2021a), ecosystem resilience (Vogel et al., 2021), and climate trends (Dorigo et al., 2012)

The baseline algorithm to retrieve SM from passive microwave observations for ESA CCI is the Land Parameter Retrieval Model (LPRM) (Owe et al., 2001). As compared to other retrieval methods which are sensor specific (Pan et al., 2014; Wigneron et al., 2000; Rodriguez-Fernandez et al., 2015), LPRM can be applied to most microwave radiometers and their frequencies. LPRM solves the zero-order radiative transfer equations and simultaneously estimates SM and the vegetation optical depth (VOD) (Mo et al., 1982). It requires the horizontal and vertical polarized brightness temperatures, surface temperature (der Schalie et al., 2016; Owe et al., 2008), and ancillary soil properties such as soil, clay contents and bulk density (Das and O'Neill, 2020) as input.

One of the input parameters to LPRM is an accurate measure of the temperature of the emitting layer (T_{eff}). Space borne microwave radiometers are capable of acquiring measurements both day and nighttime, as the sensed brightness temperature is the product of the emissivity and the effective thermodynamic temperature of the emitting layer T_{eff}. The emitting layer, or penetration depth, is the subsurface layer from which natural microwave emission occurs (Favrichon et al., 2023b). In LPRM by default, the surface temperature (T_{surf}) is required to isolate surface emissivity from observed brightness temperatures, allowing the estimation of SM, which is the function of the surface dielectric properties and its emissivity. LPRM retrieves T_{surf} by a pre-calibrated linear model using Ka-band (36.5 GHz) brightness temperatures (Holmes et al., 2009) while the SM retrieval itself is applied to observations from lower frequencies. Due to its shallower penetration depth, the Ka-band based temperature will be more representative of the top layer of the soil, than frequencies like the C-band used for SM estimation (Bindlish et al., 2017a; Yee et al., 2017).

Throughout the night, T_{surf} and T_{eff} are assumed to be at equilibrium, but daytime surface temperature observations have a substantial vertical gradient, due to strong solar heating. Hence the T_{surf} is greater than T_{eff} over the day. The Ka-band based T_{surf} is then not equal to T_{eff} from which the C-band emission occurs, causing an inequality in the sensed temperatures ultimately lowering the quality of SM retrievals (Van de Griend, 2002; Yee et al., 2017). The diurnal temperature gradient as a function of sensing depth was also recognized by (Holmes et al., 2015; Zhou et al., 2015, 2017). Additionally, Favrichon et al. (2023a) concluded that not only sensing depth, but also the different types of soil properties play an important role in the diurnal temperature gradients. Such diurnal temperature gradients could lead to distinct systematic and random errors in daytime retrievals.

https://doi.org/10.5194/egusphere-2026-6686
Preprint. Discussion started: 17 November 2026
© Author(s) 2026. CC BY 4.0 License.

Satellites specifically engineered for SM monitoring, like SMOS and SMAP, fly on a dawn/dusk orbit with 06:00 and 18:00 equator crossing times. This design aims to mitigate differences between daytime T_{surf} and T_{eff} by acquiring observations when vertical temperature gradients are minimized and the soil column is nearest to thermal equilibrium. However, sensors in noon/midnight sun-synchronous orbits, such as AMSR-E, AMSR-2, and FengYun-3B/C/D, observe the earth surface near the diurnal solar peak maximizing the thermal divergence between T_{surf} and T_{eff} (Fagerlund et al., 1970; Basharinov and Shutko, 1975). To mitigate the thermal gradient effects across daytime overpasses, Choudhury et al. (1982) introduced globally static parameters, based on physical simulations to define the relationship between T_{eff} and T_{surf} for different frequencies. This framework was later refined for the SMAP Single- and Dual-Channel Algorithms (SCA and DCA) by incorporating local bias corrections against in situ soil temperature observations to account for vegetation cover variability (Jackson, 1993; Njoku and Li, 1997). Similarly, the L-band Microwave Emission of the Biosphere (L-MEB) model for SMOS accounts for vertical temperature gradients by ingesting modeled multi-layer soil temperatures from ECMWF (Wigneron et al., 2007). While effective, these retrieval schemes remain heavily dependent on land surface models. Consequently, there is a critical need to develop independent, satellite-based methods to estimate these vertical thermal profiles. Properly accounting for the differences in soil temperatures as a function of depth facilitates the merging of global soil moisture observations from both overpasses, help future satellite mission design and the parametrization of observation error variances in data assimilation systems (Entekhabi et al., 2014; Lei et al., 2015; Gruber et al., 2019). Furthermore, correcting for the gradient in temperatures will lead to ultimately reducing systemic biases and yielding more reliable inputs for land surface models and hydrological data assimilation systems Shaoning et al. (2014); Lv et al. (2016). The here presented approach mitigates temperature gradients by using solely satellite observations, bypassing the need for the dependency and the calibration against ancillary datasets leading to a more "empirical" approach. The SM estimates derived from the proposed daytime-optimized method exhibit reduced bias compared to both reference reanalysis data and in situ measurements.

2 Materials & Methods

This section introduces the general retrieval model for SM and VOD, the methodology and the steps taken to obtain optimized daytime retrievals. Figure 1 provides an overview of the algorithmic approach followed in this study.

https://doi.org/10.5194/egusphere-2026-6686
Preprint. Discussion started: 17 November 2026
© Author(s) 2026. CC BY 4.0 License.

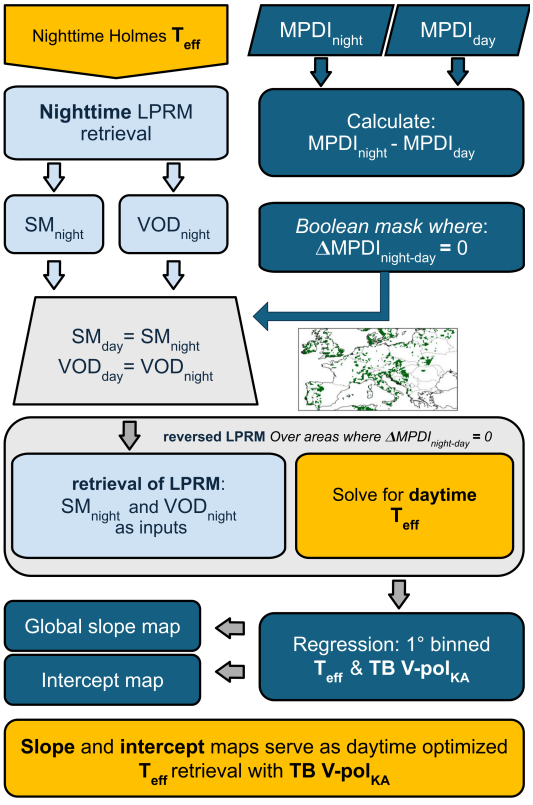


Figure 1. Workflow to obtain global regression parameters for daytime T_{eff} estimation. Variables shown include soil moisture (SM), vegetation optical depth (VOD), microwave polarization difference index (MPDI), and vertically polarized brightness temperature at Ka-band (TB V-pol$_{KA}$).

2.1 AMSR2

Microwave observations were used from the AMSR2, throughout 2024. AMSR2 onboard the GCOM-W1 satellite is on a sun-synchronous orbit with equator crossing times at 13:30 (daytime) and at 01:30 (nighttime) local solar time. AMSR2 brightness temperature observations were resampled to a fixed, 0.25°global grid using a nearest neighbor method, where output pixels were assigned the value of the geographically closest input pixel. The algorithm uses a 25 km search radius for closest neighbors. Table 1 shows the microwave bands used in this study, where C refers to the lower frequency "C1"-band on AMSR2.

https://doi.org/10.5194/egusphere-2026-6686
Preprint. Discussion started: 17 November 2026
© Author(s) 2026. CC BY 4.0 License.

Table 1. AMSR2 sensor properties. Table adapted from Imaoka et al. (2010)

Band	Center frequency (GHz)	Band width (MHz)	Beam Width (3dB, degree)	GIFOV scan × along track (kms)	Ground sampling interval (km)
C	6.9	350	1.8	35 x 62	10
Ka	36.5	1000	0.35	7 x 12	10

2.2 Land Parameter Retrieval Model

Within the ESA CCI SM project, the core radiate transfer scheme used by passive microwave radiometers is LPRM (Owe et al., 2001; Dorigo, 2026) (*in press*). LPRM relies on the zero-order radiative transfer equation, the $\tau - \omega$ model, which describes the upwelling radiation emitted by the land surface as measured above the vegetation canopy (Mo et al., 1982):

$$TB_{(P)} = T_{Soil} e_{r(P)} \Gamma + (1-\omega) T_{Canopy} (1-\Gamma) \quad + (1 - e_{r(P)})(1-\omega) T_{Canopy} (1-\Gamma)\Gamma \tag{1}$$

The first term in the above equation represents the soil component of the total radiation, as it passes through the canopy, the second term describes the upward radiation emitted directly from the canopy, the third term is the radiation emitted downward from the canopy, reflected by the soil and again attenuated by the canopy. $TB_{(P)}$ is the brightness temperature at H-or V-polarization, $e_{r(P)}$ is the rough surface emissivity, ω is the single scattering albedo and Γ is the vegetation transmissivity, which is the function of the observation angle u, and τ (VOD):

$$\Gamma = \exp\left(\frac{-\tau}{\cos(u)}\right). \tag{2}$$

A key assumption is that $T_{Soil} \approx T_{Canopy} \approx T_{surf} \approx T_{eff}$, which holds true over nighttime observations, but is less accurate during daytime. The reason behind this is the different thermal properties of vegetation and soil, thus both heat and cool at different rates during the day (Pablos et al., 2016). In LPRM by default, T_{eff} is derived using the Ka-band vertically polarized brightness temperatures (TB_{KaV}) with globally fixed regression parameters. The vertical polarization is favored as it is less sensitive to changes in SM at observations angles of 50–55°as compared to horizontal polarization. Ka frequency is used because it balances a reduced sensitivity to soil surface characteristics with a high atmospheric transmissivity (Colwell, 1983). Holmes et al. (2009) developed a generic method, that is applicable globally, with fixed slope and intercept. This effective temperature is hereinafter referred to as $T_{\mathrm{eff,Holmes}}$, and formulated as:

$$\mathrm{T_{eff,Holmes}} = 0.893\mathrm{TB_{KaV}} + 44.8 \tag{3}$$

The parameters in Eq. 3 are constant across the globe, thus they do not account for the effect of vegetation cover or sensing depth. During retrieval in LPRM, a range of soil emissivities ($e_{r(P)}$) and vegetation transmissivities ($\Gamma_{(P)}$) are iterated in Eq. 1,

https://doi.org/10.5194/egusphere-2026-6686
Preprint. Discussion started: 17 November 2026
© Author(s) 2026. CC BY 4.0 License.

as calculated from a dielectric mixing model and an analytical approach using the Microwave polarization Difference Index (MPDI) (Wang and Schmugge, 1980; Meesters et al., 2005), respectively. The model achieves convergence when the difference between the simulated and brightness temperatures observed by the satellite sensor is minimized, and thus SM and VOD are obtained.

Daytime microwave SM retrievals are complicated by differing diurnal heating rates across different soils and vegetation covers, alongside varying microwave penetration depths. This uneven heating by solar radiation creates a specific temperature gradient, making T_{surf} higher than T_{eff}. Dry soils (e.g., the Sahara and the US Midwest) are characterized by steep vertical soil temperature gradients, resulting in larger changes in temperature across the emitting layer. In contrast, more densely vegetated areas (US Southeast) exhibit a shallower temperature gradient, indicating smaller differences between T_{surf} and T_{eff} (Owe and Van de Griend, 1998). Since the default effective temperature ($T_{\text{eff, Holmes}}$) input to LPRM is based on the vertical polarization of Ka-band, it measures a very thin, top layer of the soil ranging from 1 mm (wet) to 1 cm (dry) (Holmes et al., 2009; Ulaby et al., 1986). The emitting depth for C-band, which measures at a significantly longer wavelength than Ka, can reach up to 4-5 cm, where effective soil temperature during the day is much colder integrating emissions from throughout this depth up to the surface (Wang, 1987; Wang and Choudhury, 1981). This difference between sensed surface temperature and effective temperature presents a challenge for biophysical parameter retrieval with microwaves, which is particularly pronounced in sand deserts, where C-band microwave radiation is emitted from deeper sub-surface layers (Holmes et al., 2013; Favrichon et al., 2023a). Since during the day the observed T_{surf}, is much greater than T_{eff}, the radiative transfer model in (Eq. 1) will overestimate SM retrievals (Owe and Van de Griend, 1998), as emissivity is inversely proportional to SM. Considering no vegetation, the first term in Eq. 1 with increased T_{surf} will require a lower emissivity for the soil, thus increasing the estimated moisture content. For this reason, $T_{\text{eff, Holmes}}$ can not be accurately used during both day and nighttime retrievals, therefore it must be adjusted.

Figure 5a demonstrates the bias in day-night SM caused by the thermal gradient effect: AMSR2 C-band soil moisture data using $T_{\text{eff, Holmes}}$ input, show substantially greater daytime bias than nighttime bias over bare/desert LCs (see US Midwest). Comparing the same SM retrievals to in situ measurements, from the International Soil Moisture Network (Dorigo et al., 2013, 2021b) confirms this pattern, as shown on Figure 5 (b). The day-night bias difference ($\Delta\text{Bias} = \text{Bias}_{\text{day}} - \text{Bias}_{\text{night}}$) indicates a greater positive daytime bias over semi-arid US Midwest regions than over densely vegetated regions, such as the East Coast.

2.3 Estimating daytime T_{eff} with the constant MPDI method

The challenge with daytime retrievals results from the increased degree of freedom introduced by the changing temperatures present at different soil and canopy depths. With explicit soil and canopy temperatures, Eq. 1 becomes indeterminate, with two unknowns. Thus, we propose a method that accounts for the effect of soil-vegetation interaction of T_{eff} measurements while keeping Eq. 1 determinate. The method for obtaining daytime optimized T_{eff} is based on an algebraic rearrangement of Eq. 1. The goal is to find an answer to the question: *"What effective temperature values would be required during daytime observations, to obtain target SM and VOD estimates?"*. Reversing the retrieval algorithm and using SM and VOD not as

https://doi.org/10.5194/egusphere-2026-6686
Preprint. Discussion started: 17 November 2026
© Author(s) 2026. CC BY 4.0 License.

outputs, but as inputs to the model, Eq. 1 can be reformulated to isolate the simulated daytime T_{eff} as the dependent variable. Using SM and VOD as inputs, we can simulate the theoretical T_{eff} necessary to satisfy the radiative transfer equation under daytime conditions. Luckily, quality SM and VOD observations, that remained unchanged from night to day, are available from nighttime observations (with $T_{\mathrm{eff,Holmes}}$ estimates from Eq. 3). To find regions where SM and VOD from the nighttime overpass could serve as inputs to the daytime T_{eff} simulation, the Microwave polarization Difference Index (MPDI) was used.

$$\mathrm{MPDI} = \frac{T_{\mathrm{b[V]}} - T_{\mathrm{b[H]}}}{T_{\mathrm{b[V]}} + T_{\mathrm{b[H]}}}. \tag{4}$$

MPDI can be easily calculated by dual-polarized microwave TB observations, depending only on soil dielectric constant and τ (Owe et al., 2001; Meesters et al., 2005). By combining the $\tau - \omega$ model with the assumptions that soil and canopy temperatures are equal, vegetation parameters (τ and ω) are polarization-independent, and atmospheric contributions are negligible, Meesters et al. (2005) formulated MPDI in terms of soil and vegetation emissivities. Thus, it can be assumed that if no change is observed in MPDI from night-to-day overpasses, SM and VOD also remain constant (de Jeu et al., 2026). Initial SM and VOD estimates were used from locations where $\Delta MPDI_{night-day} \simeq 0$, to solve the reversed radiative transfer model for simulated daytime T_{eff}. Pixels with MPDI < 0.01 were excluded, as these indicate dense vegetation canopies that are opaque to microwave radiation.

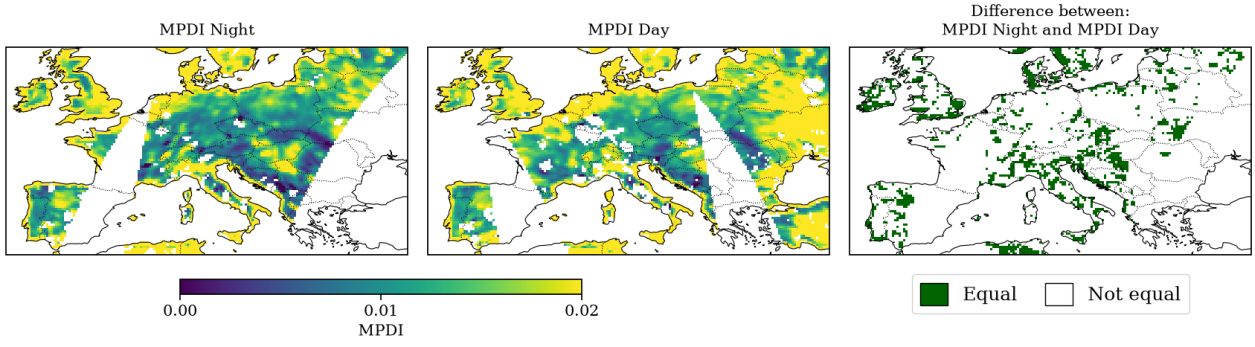


Figure 2. C-band AMSR2 day and night time MPDI, and the locations where they remain constant. 2024 May 1st

Figure 2 shows an example of day and nighttime MPDIs, as well as the observations where no change in its value was observed. Over such constant MPDI regions, SM and VOD from night overpasses were used to run LPRM in reversed order. Instead of estimating SM and VOD from dual-polarized brightness temperatures and T_{eff}, the retrieval is inverted: nighttime SM and VOD and daytime brightness temperatures are used to solve for daytime T_{eff}. The simulated daytime T_{eff} were regressed against daytime TB_{KaV} observations. Original 0.25°observations were aggregated to 1°bins, and linear regression metrics (slope, intercept) were calculated over 2024 (4 x 4 x 366 array bins). This aggregation is required to ensure the regression model has enough points to work effectively. These slope and intercept maps serve as the basis for the regression-based retrieval for the optimized daytime T_{eff}. Eq. 5 shows the formulation:

https://doi.org/10.5194/egusphere-2026-6686
Preprint. Discussion started: 17 November 2026
© Author(s) 2026. CC BY 4.0 License.

$$\mathrm{T}_{\mathrm{eff,Daytime}}(\mathbf{x}) = \alpha(\mathbf{x})\mathrm{TB}_{\mathrm{KaV}} + \beta(\mathbf{x}) \tag{5}$$

where $\mathbf{x} = (\mathrm{lat}, \mathrm{lon})$, α is the slope and β the intercept. Daytime T_{eff} was then calculated for each location using TB_{KaV} and slope and intercept as a function of latitude and longitude from the regression maps. Daytime optimized, vegetation cover dependent, regression based T_{eff} (hereafter named $T_{\mathrm{eff,optimised}}$) were obtained using Equation 5 serving as an input for the improved daytime SM estimates.

3 Results & Discussion

3.1 Global slope and intercept maps

Figure 3 shows the slope and intercept from the regression analysis (aggregated into 1°bins). The correlation showed highly linear, LC and vegetation cover dependent slopes and intercepts. Arid and semi-arid biomes (e.g., the Sahara, Arabian Desert, and Western Australia) exhibit shallower slopes and higher intercepts, whereas densely vegetated regions (e.g., the Eastern US, Central Europe, and Northern Russia) display steeper slopes and lower intercepts.

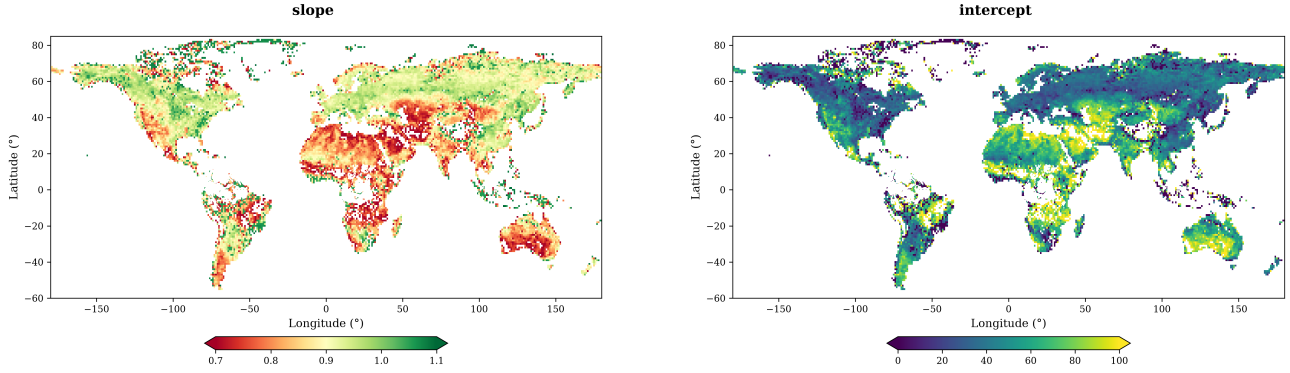


Figure 3. Resulting slope and intercept obtained by the linear regression between simulated T_{eff} and TB_{KaV} for C-band.

The difference in the retrieved T_{eff} by the standard and optimized method, is shown on Figure 4. It is clearly visible, that in general the optimized land cover regression based approach provides colder (3-5 K) temperature estimates than $T_{\mathrm{eff,Holmes}}$, over the deserts, indicating the aforementioned steep temperature gradient.

https://doi.org/10.5194/egusphere-2026-6686
Preprint. Discussion started: 17 November 2026
© Author(s) 2026. CC BY 4.0 License.

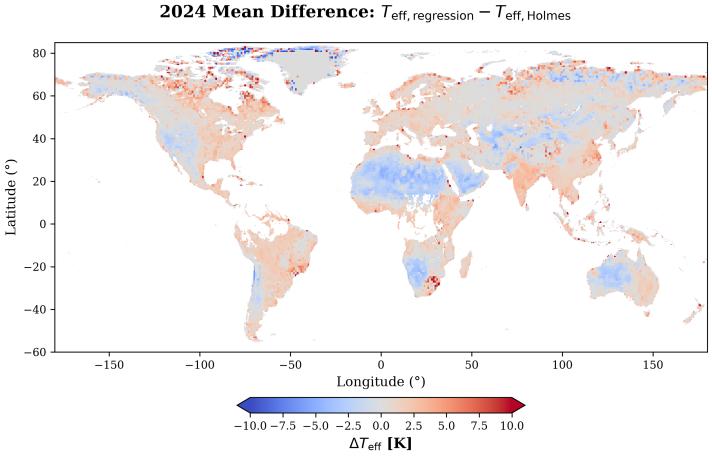


Figure 4. Mean temperature difference in 2024 between $T_{\text{eff, optimised}}$ versus $T_{\text{eff, Holmes}}$.

3.2 Comparison against reference data

LPRM was run in two configurations over 2024: one with the daytime optimized $T_{\text{eff, optimised}}$ input and one with $T_{\text{eff, Holmes}}$. Figure 6a shows the bias between these retrievals and shows that the strong vegetation cover dependence over-/underestimations have reduced drastically, as previously seen in Figure 5a. The previously observed overestimation by daytime SM estimates over arid, semi-arid regions (Sahara, Namib/Kalahari deserts, US Midwest) have been reduced, as well as over densely vegetated areas, (crop fields in India, South-East Pacific). Figure 6 shows the $T_{\text{eff, optimised}}$ input to LPRM narrows the bias distribution, aligning day and night retrievals. Using the default $T_{eff,Holmes}$ configuration, daytime C-band retrievals exhibit a distinct positive bias against nighttime estimates, with a global mean bias of $0.00131\ m^3/m^3$ and standard deviation (std) of $0.0295\ m^3/m^3$. Introducing $T_{eff,optimised}$ shifts the bias towards zero and negative values, to a mean of $-0.00659\ m^3/m^3$ and shifting the std to $-0.04\ m^3/m^3$. The change in skewness (from $0.0818\ to -3.14$) indicates, that the artificial daytime bias has been reduced.

https://doi.org/10.5194/egusphere-2026-6686
Preprint. Discussion started: 17 November 2026
© Author(s) 2026. CC BY 4.0 License.

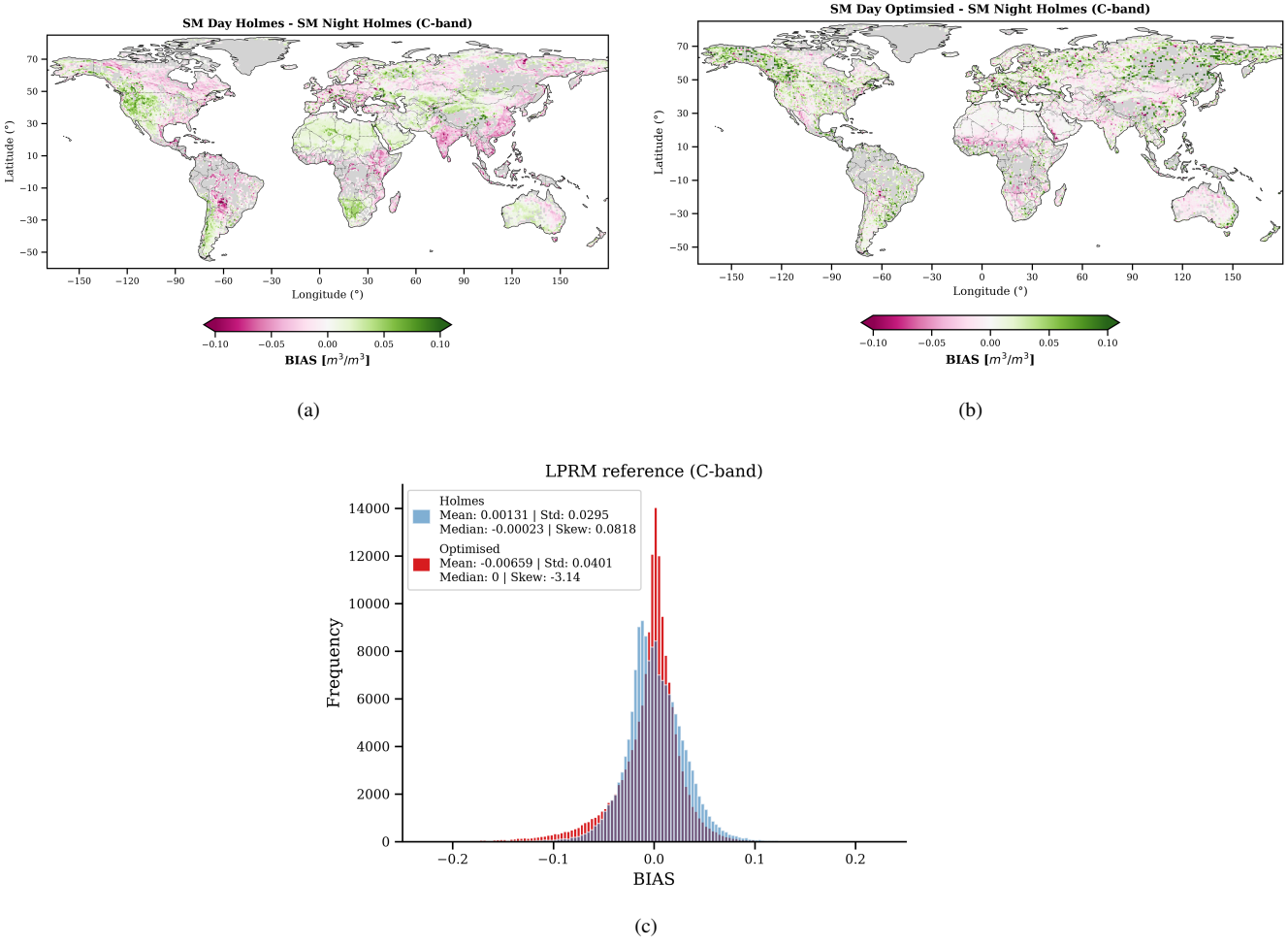
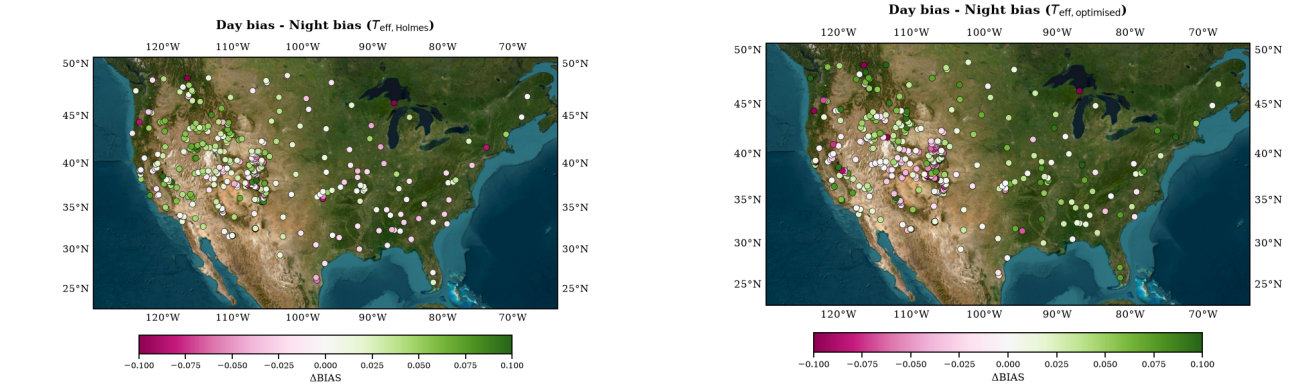


Figure 5. (a) Soil moisture (SM) retrieval biases between daytime and nighttime overpasses using the $T_{\mathrm{eff,Holmes}}$ parameterization. (b) using the $T_{\mathrm{eff,regression}}$ parameterization. (c) Corresponding histogram of bias for Holmes and Optimised methods.

https://doi.org/10.5194/egusphere-2026-6686
Preprint. Discussion started: 17 November 2026
© Author(s) 2026. CC BY 4.0 License.

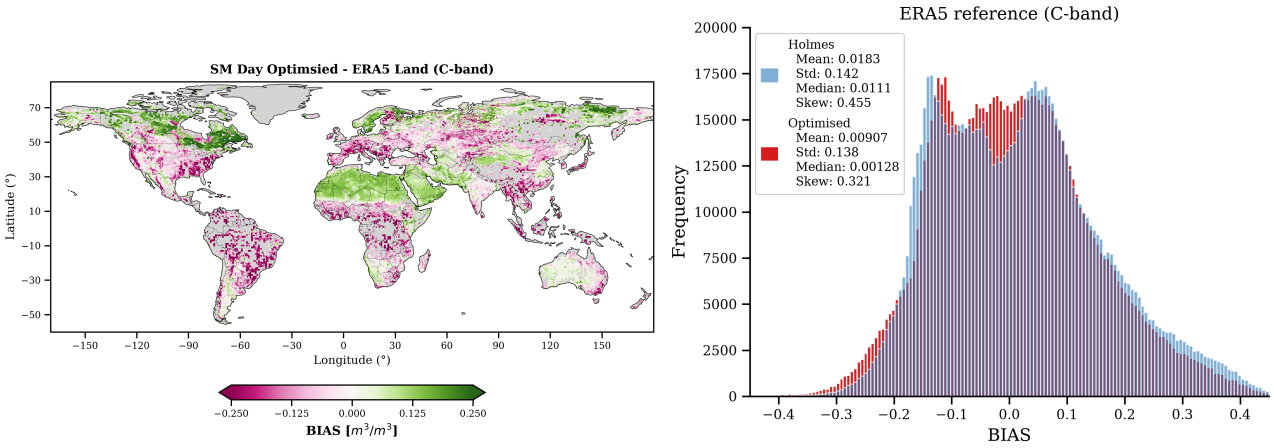


(a) (b)

Figure 6. (a) day-night bias difference ($\Delta\text{Bias} = \text{Bias}_{\text{day}} - \text{Bias}_{\text{night}}$) with respect to International Soil Moisture Network (ISMN) in situ station measurements (between 0 and 10 cm depths). Usign $T_{\text{eff, Holmes}}$ and (b) using $T_{\text{eff, optimised}}$. A land cover map over the area is shown on Figure A2. © Esri - Source: Esri, i-cubed, USDA, USGS, AEX, GeoEye, Getmapping, Aerogrid, IGN, IGP, UPR-EGP, and the GIS User Community | Powered by Esri.

The daytime SM retrievals using optimized $T_{\text{eff, optimised}}$ input were also compared to ERA5-land. The differences between the datasets are inherently higher due to the different nature of the observations (satellite vs. reanalysis). When comparing Figures 6 (a) and Figure 5 (a), it can be observed that the general direction of biases aligns, regardless of comparing to satellite or reanalysis data. Despite their different nature, biases were significantly reduced when introducing $T_{\text{eff, optimised}}$. Mean bias against ERA5-Land is reduced by more than half (from $+0.0183$ to $+0.0091$ m^3/m^3) with std also slightly decreasing (from $+0.142$ to $+0.138$ m^3/m^3). Similarly to the LPRM reference, the skewness has decreased, although not so drastically, from 0.455 to 0.321).

https://doi.org/10.5194/egusphere-2026-6686
Preprint. Discussion started: 17 November 2026
© Author(s) 2026. CC BY 4.0 License.



(a) (b)

Figure 7. (a) Bias between SM from from LPRM using $T_{eff,optimised}$ versus ERA5-Land over 2024. (b) Corresponding histogram of bias for Holmes-ERA5-Land (in Appendix) and Optimised-ERA5-Land methods.

3.3 Optimised T_{eff} inputs to LPRM

Depending on the location, the new regression parameters for $T_{\mathrm{eff,optimised}}$ estimation can be very different to the globally fixed ones in Eq. 3. However, when comparing the retrieved T_{eff} measurements using the two different methods, their magnitude differs just slightly, indicating the new regression parameters serve as a correction for the vegetation cover's sensitivity to the daytime gradients between T_{surf} and T_{eff}. Figure 3 shows steeper slopes for vegetated regions (e.g.: North Russia, Canada) but shallower gradients for sparsely vegetated areas. This indicates that T_{eff} is more sensitive to subtle changes to TB_{KaV} (or T_{surf}) in vegetated areas, because here the emitting depth of C-band is much closer to Ka (Norouzi et al., 2015, 2012). Moreover, the Ka-band is quite opaque to vegetation, and for roughly 60% of Earth, T_{surf} will represent the temperature of the vegetation canopy (Holmes et al., 2009). Conversely, the lower sensitivity indicated by shallower slopes in bare areas could be attributed to the greater difference in sensing depth between C- and Ka-bands Holmes et al. (2013). In arid regions, variations in lithological composition and soil roughness (Jiménez et al., 2010) significantly influence penetration depth-driven sensitivity, as observed in locations like the Rub' al Khali erg in the southern Arabian Peninsula or the Tibesti Mountains in the central Sahara. The slope and intercept maps show similarities to the microwave emission depth maps, presented by (Favrichon et al., 2023b), indicating that the correction for gradient between daytime T_{surf} and T_{eff} does heavily depend on vegetation cover and soil composition. The deeper penetration and, thus, the colder effective sensing temperature over deserts for C-band is clearly visible in Figure 4 (Matzler, 1998; Zhou et al., 2017). Although the work by Lv et al. (2018) relies on L-band signals which are longer wavelengths than C-band, the here presented analysis is in line with the penetration depth maps they produced.

https://doi.org/10.5194/egusphere-2026-6686
Preprint. Discussion started: 17 November 2026
© Author(s) 2026. CC BY 4.0 License.

3.4 Daytime optimization effect on SM retrieval

Accounting for thermal gradients results in noticeably lower daytime effective temperatures over bare LCs. As presented in Figure 4, the pattern is consistent with Zotta et al. (2026) and Parinussa et al. (2016), both reporting a significant overestimation of uncorrected temperatures across drier regions. The reduction in bias in daytime SM is attributed to the colder $T_{\text{eff, optimised}}$ values compared to $T_{\text{eff, Holmes}}$ over deserts, as the deeper sensing depths of the C-band require a lower temperature input. Conversely, a warmer $T_{\text{eff, optimised}}$ is needed over vegetated regions, suggesting that while $T_{\text{eff, Holmes}}$ serves as a practical generic solution across all land covers, it lacks LC specific optimization (Holmes et al., 2009). Furthermore, the direction of these bias changes achieved by introducing the daytime regression parameters for T_{eff} estimation is consistent with the $T_{\text{eff, Holmes}}$ temperature difference maps in Figure 4. This alignment indicates that the underlying issue is dependent on sensing depth and vegetation cover (Lei et al., 2015; Parinussa et al., 2011), and thus the optimized $T_{\text{eff, optimised}}$ compensate for this. Values are more tightly clustered around zero (Figure 6c), indicating a global bias reduction. Daytime optimized SM retrievals were also compared against in situ validation data (Table A1), where notable changes were observed on the magnitude of mean bias. For the daytime optimized retrievals bias was reduced from $-0.00805\ m^3/m^3$ to $-0.0000172\ m^3/m^3$, while other metrics remained invariant. The higher bias between microwave and reanalysis based SM estimates was also reported by (Zhu et al., 2025; Ling et al., 2021), with slight negative bias towards LPRM based methods. When evaluated against LPRM references, bias reduction occurs primarily in areas of dense vegetation, contrasting with the more generic reduction across all LCs when comparing against ERA5.

3.5 Limitations

The presented method proves as a bias correction for daytime SM estimation, though, care must be taken, as not all satellites suitable for LPRM-based retrievals fly on the same type of orbit as the here used AMSR2. With fixed equatorial overpass times of 01:30 and 13:30, AMSR2 always captures the same solar illuminance conditions. Further research needs to address the effect of the irregular overpass times of satellites like GPM or TRMM (Liu et al., 2012; Smith et al., 2007). Because these satellites operate on non-sun-synchronous orbits, their local observation times over any given location continuously shift throughout the year. This means that their observed difference between T_{eff} and T_{surf} will vary drastically. Therefore, they are unable to use the presented regression maps, to account for the diurnal temperature gradient. Satellites with overpass times radically different to AMSR2, will also require further calibration.

While aggregating observations into 1°spatial bins was essential for robust parameter estimation, the scale mismatch with the 0.25°gridded observations introduces uncertainties associated with sub-pixel land surface heterogeneity. Such heterogeneity and dense land covers both impact daytime regression parameter estimation and thus final soil moisture retrieval accuracies (Lamichhane et al., 2025).

https://doi.org/10.5194/egusphere-2026-6686
Preprint. Discussion started: 17 November 2026
© Author(s) 2026. CC BY 4.0 License.

4 Conclusions

This study presents a method to correct for daytime biases in passive microwave SM retrievals, caused by vertical temperature gradients in soils, between the top surface and deeper effective emitting depths. By using MPDI values that remained constant from night to day, C-band SM and VOD observations could be detected globally where they remained invariant. Over locations where no change in MPDI was detected, nighttime SM and VOD could be used as an input to LPRM. By running the LPRM radiative transfer equation in a reversed manner, the theoretical effective temperature could be simulated, for daytime conditions. Correlating these simulated temperatures to Ka-band vertically polarised brightness temperatures yielded, global, vegetation cover dependent regression metrics namely slope and intercept, which proved to be dependent on vegetation cover. Using the obtained regression coefficients, effective temperatures optimized for daytime retrievals were derived using AMSR2 observations. Implementing the optimized temperatures in LPRM, reduces daytime SM biases across both arid and vegetated regions, aligning the agreement with nighttime references and ERA5-Land data. The presented methodology will greatly enhance the overall quality of merged SM products, such as ESA CCI, as large portions of the data is sensed over daytime, for which biases are now reduced. Additionally, the here presented method plays an important role in the quality of the SUB-DAILY product too, which is specifically tailored for global, diurnal SM assessment with a 12-hourly temporal resolution (Lems et al., 2026). Moreover, thanks to the parallel retrieval of VOD alongside SM, daytime retrievals could also serve as improvements on that front. Further research will address L-band only sensors (e.g., SMOS, SMAP), which lack a Ka-band channel capable of estimating T_{eff}, as well as satellites on non-sun-synchronous orbits with irregular overpass times.

Appendix A

A1

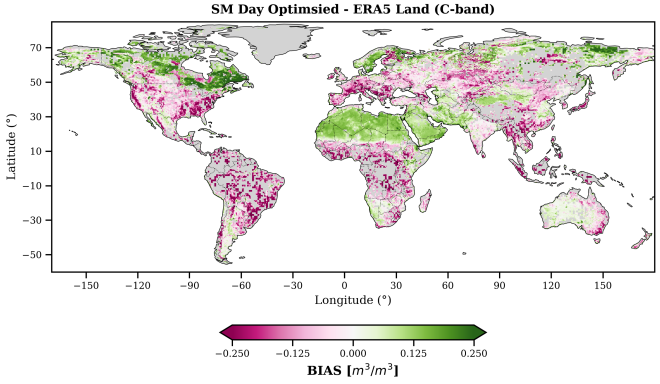


Figure A1. Bias between SM from from LPRM using $T_{eff,Holmes}$ versus ERA5-Land over 2024.

https://doi.org/10.5194/egusphere-2026-6686
Preprint. Discussion started: 17 November 2026
© Author(s) 2026. CC BY 4.0 License.

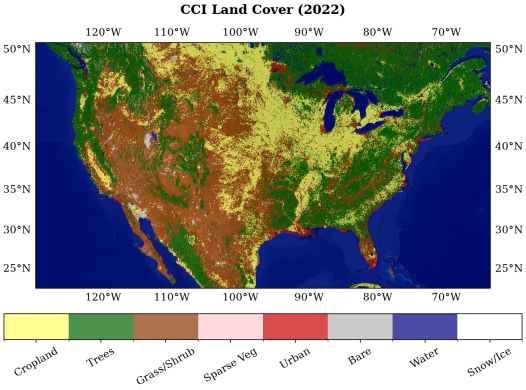


Figure A2. CCI Land Cover 2022 classes (Lamarche et al., 2017).

Table A1. Validation statistics when comparing C-band SM obtained using $T_{eff,Holmes}$ and $T_{eff,optimised}$ to ISMN data over 2024.

	SM $T_{eff,Holmes}$			SM $T_{eff,optimised}$		
Metric	Mean	Median	IQ range	Mean	Median	IQ range
# observations	40.81	0	0	41.2	0	0
Pearson's r	0.44	0.37	0.37	0.43	0.37	0.35
Spearman's ρ	0.42	0.35	0.39	0.41	0.35	0.38
Root-mean-square deviation in m^3/m^3	0.14	0.12	0.0799	0.14	0.12	0.0848
Bias in m^3/m^3	-0.00805	-0.00845	0.15	-0.0000172	-0.00859	0.16
Unbiased root-mean-square deviation in m^3/m^3	0.0814	0.0789	0.0342	0.0833	0.0794	0.0323
Mean square error in $(m^3/m^3)^2$	0.0224	0.0144	0.0207	0.0253	0.0156	0.0227
Mean square error correlation in $(m^3/m^3)^2$	0.00583	0.00494	0.00477	0.00611	0.00513	0.00486
Mean square error bias in $(m^3/m^3)^2$	0.0149	0.00587	0.0175	0.0174	0.0064	0.0201
Mean square error variance in $(m^3/m^3)^2$	0.00167	0.000632	0.00172	0.00176	0.000603	0.00174
Residual sum of squares in $(m^3/m^3)^2$	3.82	2.28	3.37	4.41	2.51	3.79
Validation errors	5.3	7	0	5.29	7	0

Data Availability Statement

Not applicable.

Author contributions. **D.K.D.** - Conceptualization, Methodology, Software, Writing - Original Draft. **R.d.J.** - Conceptualization, Methodology, Writing - Original Draft. **C.M.** - Software, Writing - Review & Editing. **R.M.Z** - Conceptualization, Writing - Review & Editing. **N.F.B** -

https://doi.org/10.5194/egusphere-2026-6686
Preprint. Discussion started: 17 November 2026
© Author(s) 2026. CC BY 4.0 License.

Conceptualization, Writing - Review & Editing. **W.A.D.** Conceptualization, Writing - Review & Editing, Supervision, Project administration, Funding acquisition

Acknowledgements. ESA CCI Soil Moisture has received funding from the European Space Agency (ESRIN Contract No: 4000126684/19/I-NB).

https://doi.org/10.5194/egusphere-2026-6686
Preprint. Discussion started: 17 November 2026
© Author(s) 2026. CC BY 4.0 License.

References

Basharinov, A. Y. and Shutko, A.: Simulation studies of the SHF radiation characteristics of soils under moist conditions, Simulation studies of the SHF radiation characteristics of soils under moist conditions NASA Transl. into ENGLISH of"" Modelnyye Issledovaniya SVCh Radiatsionnykh Kharacteristik Pochvo-Gruntov v Usloviyakh Uvlazhneniya"(unpublished report) Moscow, p. 1, 1975.

Bindlish, R., Cosh, M. H., Jackson, T. J., Koike, T., Fujii, H., Chan, S. K., Asanuma, J., Berg, A., Bosch, D. D., Caldwell, T., et al.: GCOM-W AMSR2 soil moisture product validation using core validation sites, IEEE Journal of selected topics in applied earth observations and remote sensing, 11, 209–219, 2017a.

Bindlish, R., Cosh, M. H., Jackson, T. J., Koike, T., Fujii, H., Chan, S. K., Asanuma, J., Berg, A., Bosch, D. D., Caldwell, T., et al.: GCOM-W AMSR2 soil moisture product validation using core validation sites, IEEE Journal of selected topics in applied earth observations and remote sensing, 11, 209–219, 2017b.

Choudhury, B., Schmugge, T., and Mo, T.: A parameterization of effective soil temperature for microwave emission, Journal of Geophysical Research: Oceans, 87, 1301–1304, 1982.

Colwell, R. N.: Manual of remote sensing, Amer. Soc. of Photogrammetry, 1983.

Das, N. and O'Neill, P.: Soil Moisture Active Passive (SMAP) ancillary data report soil attributes - version B, Jet Propulsion Lab., California Inst. of Technol., Pasadena, 2020.

de Jeu, R., Steele-Dunne, S. S., Lang, T., Amiot, C. G., Klein, M., Eble, M., and Miralles, D. G.: Using the Angular Dependence of the Polarization Ratio to Analyze Aircraft Passive Microwave Measurements Over Land, IEEE Transactions on Geoscience and Remote Sensing, 64, 1–15, https://doi.org/10.1109/TGRS.2026.3657427, 2026.

der Schalie, R., Kerr, Y., Wigneron, J., Rodríguez-Fernández, N., Al-Yaari, A., and Jeu, R.: Global SMOS Soil Moisture Retrievals from The Land Parameter Retrieval Model, International Journal of Applied Earth Observation and Geoinformation, 45, 125–134, https://doi.org/https://doi.org/10.1016/j.jag.2015.08.005, advances in the Validation and Application of Remotely Sensed Soil Moisture - Part 1, 2016.

Dorigo, W.: ESA CCI SM v9.2: global satellite soil moisture observations from 1978 to present, in press, 2026.

Dorigo, W., de Jeu, R., Chung, D., Parinussa, R., Liu, Y., Wagner, W., and Fernández-Prieto, D.: Evaluating global trends (1988–2010) in harmonized multi-satellite surface soil moisture, Geophysical Research Letters, 39, https://doi.org/https://doi.org/10.1029/2012GL052988, 2012.

Dorigo, W., Wagner, W., Albergel, C., Albrecht, F., Balsamo, G., Brocca, L., Chung, D., Ertl, M., Forkel, M., Gruber, A., Haas, E., Hamer, P. D., Hirschi, M., Ikonen, J., de Jeu, R., Kidd, R., Lahoz, W., Liu, Y. Y., Miralles, D., Mistelbauer, T., Nicolai-Shaw, N., Parinussa, R., Pratola, C., Reimer, C., van der Schalie, R., Seneviratne, S. I., Smolander, T., and Lecomte, P.: ESA CCI Soil Moisture for improved Earth system understanding: State-of-the art and future directions, Remote Sensing of Environment, 203, 185–215, https://doi.org/https://doi.org/10.1016/j.rse.2017.07.001, earth Observation of Essential Climate Variables, 2017.

Dorigo, W., Dietrich, S., Aires, F., Brocca, L., Carter, S., Cretaux, J.-F., Dunkerley, D., Enomoto, H., Forsberg, R., Güntner, A., Hegglin, M. I., Hollmann, R., Hurst, D. F., Johannessen, J. A., Kummerow, C., Lee, T., Luojus, K., Looser, U., Miralles, D. G., Pellet, V., Recknagel, T., Vargas, C. R., Schneider, U., Schoeneich, P., Schröder, M., Tapper, N., Vuglinsky, V., Wagner, W., Yu, L., Zappa, L., Zemp, M., and Aich, V.: Closing the Water Cycle from Observations across Scales: Where Do We Stand?, Bulletin of the American Meteorological Society, 102, E1897 – E1935, https://doi.org/10.1175/BAMS-D-19-0316.1, 2021a.

https://doi.org/10.5194/egusphere-2026-6686
Preprint. Discussion started: 17 November 2026
© Author(s) 2026. CC BY 4.0 License.

Dorigo, W., Himmelbauer, I., Aberer, D., Schremmer, L., Petrakovic, I., Zappa, L., Preimesberger, W., Xaver, A., Annor, F., Ardö, J., Baldocchi, D., Bitelli, M., Blöschl, G., Bogena, H., Brocca, L., Calvet, J.-C., Camarero, J. J., Capello, G., Choi, M., Cosh, M. C., van de Giesen, N., Hajdu, I., Ikonen, J., Jensen, K. H., Kanniah, K. D., de Kat, I., Kirchengast, G., Kumar Rai, P., Kyrouac, J., Larson, K., Liu, S., Loew, A., Moghaddam, M., Martínez Fernández, J., Mattar Bader, C., Morbidelli, R., Musial, J. P., Osenga, E., Palecki, M. A., Pellarin, T., Petropoulos, G. P., Pfeil, I., Powers, J., Robock, A., Rüdiger, C., Rummel, U., Strobel, M., Su, Z., Sullivan, R., Tagesson, T., Varlagin, A., Vreugdenhil, M., Walker, J., Wen, J., Wenger, F., Wigneron, J. P., Woods, M., Yang, K., Zeng, Y., Zhang, X., Zreda, M., Dietrich, S., Gruber, A., van Oevelen, P., Wagner, W., Scipal, K., Drusch, M., and Sabia, R.: The International Soil Moisture Network: serving Earth system science for over a decade, Hydrology and Earth System Sciences, 25, 5749–5804, https://doi.org/10.5194/hess-25-5749-2021, 2021b.

Dorigo, W. A., Xaver, A., Vreugdenhil, M., Gruber, A., Hegyiova, A., Sanchis-Dufau, A. D., Zamojski, D., Cordes, C., Wagner, W., and Drusch, M.: Global automated quality control of in situ soil moisture data from the International Soil Moisture Network, Vadose Zone Journal, 12, 1–21, 2013.

Du, J., Kimball, J. S., Jones, L. A., Kim, Y., Glassy, J., and Watts, J. D.: A global satellite environmental data record derived from AMSR-E and AMSR2 microwave Earth observations, Earth System Science Data, 9, 791–808, 2017.

Entekhabi, D., Njoku, E. G., O'Neill, P. E., Kellogg, K. H., Crow, W. T., Edelstein, W. N., Entin, J. K., Goodman, S. D., Jackson, T. J., Johnson, J., Kimball, J., Piepmeier, J. R., Koster, R. D., Martin, N., McDonald, K. C., Moghaddam, M., Moran, S., Reichle, R., Shi, J. C., Spencer, M. W., Thurman, S. W., Tsang, L., and Van Zyl, J.: The Soil Moisture Active Passive (SMAP) Mission, Proceedings of the IEEE, 98, 704–716, https://doi.org/10.1109/JPROC.2010.2043918, 2010.

Entekhabi, D., Yueh, S., O'Neill, P. E., Kellogg, K. H., Allen, A., Bindlish, R., Brown, M., Chan, S., Colliander, A., Crow, W. T., Das, N., De Lannoy, G., Dunbar, R. S., Edelstein, W. N., Entin, J. K., Escobar, V., Goodman, S. D., Jackson, T. J., Jai, B., Johnson, J., Kim, E., Kim, S., Kimball, J., Koster, R. D., Leon, A., McDonald, K. C., Moghaddam, M., Mohammed, P., Moran, S., Njoku, E. G., Piepmeier, J. R., Reichle, R., Rogez, F., Shi, J. C., Spencer, M. W., Thurman, S. W., Tsang, L., Van Zyl, J., Weiss, B., and West, R.: SMAP Handbook: Soil Moisture Active Passive – Mapping Soil Moisture and Freeze/Thaw from Space, JPL Publication JPL 400-1567, Jet Propulsion Laboratory, California Institute of Technology, Pasadena, CA, 2014.

Fagerlund, E., Kleman, B., Sellin, L., and Svensson, H.: Physical studies of nature by thermal mapping, Earth-Science Reviews, 6, 169–180, https://doi.org/https://doi.org/10.1016/0012-8252(70)90023-1, 1970.

Favrichon, S., Prigent, C., Jimenez, C., and Vogt, R.: Global mapping of microwave emissivity and emitting depth in arid areas using GMI observations, Earth and Space Science, 10, e2022EA002 756, 2023a.

Favrichon, S., Prigent, C., Jimenez, C., and Vogt, R.: Global mapping of microwave emissivity and emitting depth in arid areas using GMI observations, Earth and Space Science, 10, e2022EA002 756, 2023b.

Gruber, A., Scanlon, T., van der Schalie, R., Wagner, W., and Dorigo, W.: Evolution of the ESA CCI Soil Moisture climate data records and their underlying merging methodology, Earth System Science Data, 11, 717–739, 2019.

Hirschi, M., Stradiotti, P., Crezee, B., Dorigo, W., and Seneviratne, S. I.: Potential of long-term satellite observations and reanalysis products for characterising soil drying: trends and drought events, Hydrology and Earth System Sciences, 29, 397–425, 2025.

Holmes, T., Crow, W., and Hain, C.: Spatial patterns in timing of the diurnal temperature cycle, Hydrology and Earth System Sciences, 17, 3695–3706, 2013.

Holmes, T., Crow, W., Hain, C., Anderson, M., and Kustas, W.: Diurnal temperature cycle as observed by thermal infrared and microwave radiometers, Remote Sensing of Environment, 158, 110–125, 2015.

https://doi.org/10.5194/egusphere-2026-6686
Preprint. Discussion started: 17 November 2026
© Author(s) 2026. CC BY 4.0 License.

Holmes, T. R. H., De Jeu, R. A. M., Owe, M., and Dolman, A. J.: Land surface temperature from Ka band (37 GHz) passive microwave observations, Journal of Geophysical Research: Atmospheres, 114, https://doi.org/https://doi.org/10.1029/2008JD010257, 2009.

Imaoka, K., Kachi, M., Kasahara, M., Ito, N., Nakagawa, K., and Oki, T.: Instrument performance and calibration of AMSR-E and AMSR2, International archives of the photogrammetry, remote sensing and spatial information science, 38, 13–18, 2010.

Jackson, T. J.: III. Measuring surface soil moisture using passive microwave remote sensing, Hydrological processes, 7, 139–152, 1993.

Jiménez, C., Catherinot, J., Prigent, C., and Roger, J.: Relations between geological characteristics and satellite-derived infrared and microwave emissivities over deserts in northern Africa and the Arabian Peninsula, Journal of Geophysical Research: Atmospheres, 115, 2010.

Kerr, Y. H., Waldteufel, P., Wigneron, J.-P., Delwart, S., Cabot, F., Boutin, J., Escorihuela, M.-J., Font, J., Reul, N., Gruhier, C., Juglea, S. E., Drinkwater, M. R., Hahne, A., Martín-Neira, M., and Mecklenburg, S.: The SMOS Mission: New Tool for Monitoring Key Elements ofthe Global Water Cycle, Proceedings of the IEEE, 98, 666–687, https://doi.org/10.1109/JPROC.2010.2043032, 2010.

Lamarche, C., Santoro, M., Bontemps, S., d'Andrimont, R., Radoux, J., Giustarini, L., Brockmann, C., Wevers, J., Defourny, P., and Arino, O.: Compilation and validation of SAR and optical data products for a complete and global map of inland/ocean water tailored to the climate modeling community, Remote Sensing, 9, 36, 2017.

Lamichhane, M., Mehan, S., and Mankin, K. R.: Soil moisture prediction using remote sensing and machine learning algorithms: A review on progress, challenges, and opportunities, Remote Sensing, 17, 2397, 2025.

Lei, F., Crow, W. T., Shen, H., Parinussa, R. M., and Holmes, T. R.: The impact of local acquisition time on the accuracy of microwave surface soil moisture retrievals over the contiguous United States, Remote Sensing, 7, 13 448–13 465, 2015.

Lems, J., Moldenhauer, C., and Dorigo, W. A.: ESA CCI SM SUB-DAILY Long-term Climate Data Record of sub-daily Soil Moisture from merged multi- satellite observations, https://doi.org/10.48436/939n8-zg244, 2026.

Ling, X., Huang, Y., Guo, W., Wang, Y., Chen, C., Qiu, B., Ge, J., Qin, K., Xue, Y., and Peng, J.: Comprehensive evaluation of satellite-based and reanalysis soil moisture products using in situ observations over China, Hydrology and Earth System Sciences, 25, 4209–4229, 2021.

Liu, Z., Ostrenga, D., Teng, W., and Kempler, S.: Tropical Rainfall Measuring Mission (TRMM) precipitation data and services for research and applications, Bulletin of the American Meteorological Society, 93, 1317–1325, 2012.

Lv, S., Zeng, Y., Wen, J., and Su, Z.: A reappraisal of global soil effective temperature schemes, Remote sensing of environment, 183, 144–153, 2016.

Lv, S., Zeng, Y., Wen, J., Zhao, H., and Su, Z.: Estimation of penetration depth from soil effective temperature in microwave radiometry, Remote sensing, 10, 519, 2018.

Matzler, C.: Microwave permittivity of dry sand, IEEE Transactions on Geoscience and Remote Sensing, 36, 317–319, https://doi.org/10.1109/36.655342, 1998.

Meesters, A. G., De Jeu, R. A., and Owe, M.: Analytical derivation of the vegetation optical depth from the microwave polarization difference index, IEEE Geoscience and Remote Sensing Letters, 2, 121–123, 2005.

Meng, X., Yang, Y., Zeng, J., Peng, J., and Hu, J.: Improvement of AMSR2 soil moisture retrieval using a soil-vegetation temperature decomposition algorithm, IEEE Geoscience and Remote Sensing Letters, 19, 1–5, 2022.

Mo, T., Choudhury, B. J., Schmugge, T. J., Wang, J. R., and Jackson, T. J.: A model for microwave emission from vegetation-covered fields, Journal of Geophysical Research: Oceans, 87, 11 229–11 237, https://doi.org/https://doi.org/10.1029/JC087iC13p11229, 1982.

Njoku, E. G. and Li, L.: Retrieval of land surface parameters using passive microwave measurements at 6 to 18 GHz, 1997.

https://doi.org/10.5194/egusphere-2026-6686
Preprint. Discussion started: 17 November 2026
© Author(s) 2026. CC BY 4.0 License.

Norouzi, H., Rossow, W., Temimi, M., Prigent, C., Azarderakhsh, M., Boukabara, S., and Khanbilvardi, R.: Using microwave brightness temperature diurnal cycle to improve emissivity retrievals over land, Remote sensing of environment, 123, 470–482, 2012.

Norouzi, H., Temimi, M., AghaKouchak, A., Azarderakhsh, M., Khanbilvardi, R., Shields, G., and Tesfagiorgis, K.: Inferring land surface parameters from the diurnal variability of microwave and infrared temperatures, Physics and Chemistry of the Earth, Parts A/B/C, 83, 28–35, 2015.

Owe, M. and Van de Griend, A. A.: Comparison of soil moisture penetration depths for several bare soils at two microwave frequencies and implications for remote sensing, Water resources research, 34, 2319–2327, 1998.

Owe, M., de Jeu, R., and Walker, J.: A methodology for surface soil moisture and vegetation optical depth retrieval using the microwave polarization difference index, IEEE Transactions on Geoscience and Remote Sensing, 39, 1643–1654, https://doi.org/10.1109/36.942542, 2001.

Owe, M., de Jeu, R., and Holmes, T.: Multisensor historical climatology of satellite-derived global land surface moisture, Journal of Geophysical Research: Earth Surface, 113, https://doi.org/https://doi.org/10.1029/2007JF000769, 2008.

Pablos, M., Piles, M., Sánchez, N., Vall-llossera, M., Martínez-Fernández, J., and Camps, A.: Impact of day/night time land surface temperature in soil moisture disaggregation algorithms, European Journal of Remote Sensing, 49, 899–916, 2016.

Pan, M., Sahoo, A. K., and Wood, E. F.: Improving soil moisture retrievals from a physically-based radiative transfer model, Remote Sensing of Environment, 140, 130–140, 2014.

Parinussa, R., Holmes, T., Yilmaz, M., and Crow, W.: The impact of land surface temperature on soil moisture anomaly detection from passive microwave observations, Hydrology and Earth System Sciences, 15, 3135–3151, 2011.

Parinussa, R. M., De Jeu, R. A., Van der Schalie, R., Crow, W. T., Lei, F., and Holmes, T. R.: A quasi-global approach to improve day-time satellite surface soil moisture anomalies through the land surface temperature input, Climate, 4, 50, 2016.

Rodriguez-Fernandez, N. J., Aires, F., Richaume, P., Kerr, Y. H., Prigent, C., Kolassa, J., Cabot, F., Jimenez, C., Mahmoodi, A., and Drusch, M.: Soil moisture retrieval using neural networks: Application to SMOS, IEEE Transactions on Geoscience and Remote Sensing, 53, 5991–6007, 2015.

Shaoning, L., Wen, J., Zeng, Y., Tian, H., and Su, Z.: An improved two-layer algorithm for estimating effective soil temperature in microwave radiometry using in situ temperature and soil moisture measurements, Remote sensing of environment, 152, 356–363, 2014.

Smith, E. A., Asrar, G., Furuhama, Y., Ginati, A., Mugnai, A., Nakamura, K., Adler, R. F., Chou, M.-D., Desbois, M., Durning, J. F., et al.: International global precipitation measurement (GPM) program and mission: An overview, Measuring precipitation from space: EURAINSAT and the future, pp. 611–653, 2007.

Ulaby, F. T., Moore, R. K., and Fung, A. K.: Microwave remote sensing: Active and passive. Volume 3 - From theory to applications, 3, 41 708, 1986.

Van de Griend, A. A.: The effective thermodynamic temperature of the emitting surface at 6.6 GHz and consequences for soil moisture monitoring from space, IEEE transactions on geoscience and remote sensing, 39, 1673–1679, 2002.

van der Schalie, R., van der Vliet, M., Albergel, C., Dorigo, W., Wolski, P., and de Jeu, R.: Characterizing natural variability in complex hydrological systems using passive microwave-based climate data records: a case study for the Okavango Delta, Hydrology and Earth System Sciences, 26, 3611–3627, https://doi.org/10.5194/hess-26-3611-2022, 2022.

Vogel, J., Paton, E., and Aich, V.: Seasonal ecosystem vulnerability to climatic anomalies in the Mediterranean, Biogeosciences Discussions, 2021, 1–30, 2021.

https://doi.org/10.5194/egusphere-2026-6686
Preprint. Discussion started: 17 November 2026
© Author(s) 2026. CC BY 4.0 License.

Wang, J. and Choudhury, B.: Remote sensing of soil moisture content, over bare field at 1.4 GHz frequency, Journal of Geophysical Research: Oceans, 86, 5277–5282, 1981.

Wang, J. R.: Microwave Emission from Smooth Bare Fields and Soil Moisture Sampling Depth, IEEE Transactions on Geoscience and Remote Sensing, GE-25, 616–622, https://doi.org/10.1109/TGRS.1987.289840, 1987.

Wang, J. R. and Schmugge, T. J.: An empirical model for the complex dielectric permittivity of soils as a function of water content, IEEE Transactions on Geoscience and remote sensing, pp. 288–295, 1980.

Wigneron, J.-P., Waldteufel, P., Chanzy, A., Calvet, J.-C., and Kerr, Y.: Two-dimensional microwave interferometer retrieval capabilities over land surfaces (SMOS mission), Remote Sensing of Environment, 73, 270–282, 2000.

Wigneron, J.-P., Kerr, Y., Waldteufel, P., Saleh, K., Escorihuela, M.-J., Richaume, P., Ferrazzoli, P., De Rosnay, P., Gurney, R., Calvet, J.-C., et al.: L-band Microwave Emission of the Biosphere (L-MEB) Model: Description and calibration against experimental data sets over crop fields, Remote Sensing of Environment, 107, 639–655, 2007.

Wu, B., Wang, Y., Zou, C.-Z., Li, R., Liu, S., Liu, G., and Fu, Y.: A fundamental climate data record derived from AMSR-E, MWRI, and AMSR2, IEEE Transactions on Geoscience and Remote Sensing, 58, 5450–5461, 2020.

Yee, M. S., Walker, J. P., Rüdiger, C., Parinussa, R. M., Koike, T., and Kerr, Y. H.: A comparison of SMOS and AMSR2 soil moisture using representative sites of the OzNet monitoring network, Remote Sensing of Environment, 195, 297–312, 2017.

Zhou, J., Dai, F., Zhang, X., Zhao, S., and Li, M.: Developing a temporally land cover-based look-up table (TL-LUT) method for estimating land surface temperature based on AMSR-E data over the Chinese landmass, International Journal of Applied Earth Observation and Geoinformation, 34, 35–50, 2015.

Zhou, J., Zhang, X., Zhan, W., Göttsche, F.-M., Liu, S., Olesen, F.-S., Hu, W., and Dai, F.: A thermal sampling depth correction method for land surface temperature estimation from satellite passive microwave observation over barren land, IEEE Transactions on Geoscience and Remote Sensing, 55, 4743–4756, 2017.

Zhu, Z., Feng, M., Cornelis, W., Miralles, D. G., Zeng, Z., Chen, Y., Yang, Z., Zou, S., Liu, Y., De Maeyer, P., et al.: Global soil moisture dynamics since 1980: datasets biases, trends, and science-informed selection, Science Bulletin, 70, 4253–4262, 2025.

Zotta, R.-M., De Jeu, R., Bader, N. F., Frederikse, T., and Dorigo, W.: Improving AMSR2 vegetation optical depth retrievals via land parameter retrieval model parameter optimisation, Remote Sensing of Environment, 335, 115 286, 2026.